

A Deep Convolutional Extreme Machine Learning Classification Method To Detect Bone Cancer From Histopathological Images

D. Anand¹, G. Arulselvi², G.N. Balaji^{*3}, G Rajesh Chandra⁴

Submitted: 10/09/2022

Accepted: 20/12/2022

Abstract

The histopathology process remains traditional in nature. Additionally, the physical process of pathologists could deal with solely restricted subjects because of extended phases. This physical process might misguide the physicians when there remain mass subjects to diagnose because of limited time and the nature of complex illnesses such as bone cancer. Addressing this study in digital histopathology remains significant by evolving computer-aided instruments for detection. Bone framework intricacy remains the chief cause to be a gray research field. Comprehension and investigation of the disparate extent of bone anatomy would serve the requirement for building study in automation. To classify the density tumor Computer-aided diagnosis systems have been developed, having as a major challenge to define the features that better represent the images to classify. To overcome the problem, this paper aims to develop a Convolutional Extreme Learning Machine (DC-ELM) algorithm for the assessment of cancer type based on analyzing histopathology images. A fusion of five important classifiers is chosen for our method. In the framework proposed, only by utilizing the karhunenloeve extraction technique, we extract such and such features of the image and, thus, for differentiation of healthy and unhealthy bone regions.

These extracted features are fed to machine learning architecture with the prediction for achieving better accuracy. As a result, the suggested DC-ELM algorithm achieves 97.27% accuracy.

Keywords – bone cancer, histopathology, classification, machine learning, ensemble classifier.

1. Introduction

Uncontrollable dividing of cells within a bone causes the development of bone cancers, developing a lump of atypical tissue. There remain 2 kinds of bone cancers – Non-cancerous (Benign) and Cancerous (Malignant). Absolutely sharp bone cancer diagnosis procedure remains significant in various applications of medical imaging. It helps in planning for early treatment, evaluation of therapy, etc. Doctors need great accuracy in analyzing bone cancer from imaging investigations, for quick bone cancer detection leads generally to more efficient treatment as well as to reduce chances of disabilities [1]. Radiologists sometimes misdiagnose due to the difficulties they come across but the process of image processing strategies can

sequently help the sharp radiologists by far with their diagnosis of bone cancer.

Histological biopsy tests, X-ray tests, and magnetic resonance images remain important detection of osteosarcoma. Presently, the detection of this incorporates comprehensive history taking and physiological investigations [4]. The posing signs generally comprise deep-seated, consistent, nagging pain, and edema in the affected place. Pain within several regions might presage skeletal metastasis; hence, they must be examined properly [5]. Past the investigation, the criterion researches for analysis of prospective osteosarcoma through lab tests, an X-ray of the completely afflicted bone, a magnetic resonance imaging (MRI) scan of the complete afflicted bone, a chest X-ray, a chest computed tomography (CT) scan, a head-to-toe technetium bone scan, and a percutaneous image-guided biopsy [6]. Even though the biopsy-related methodologies could efficiently find the malignancy, constraints within histological-guided biopsies and MRI scans possess restricted diagnosing ability. Furthermore, the histological samples' groundwork remains long-drawn-out. As an instance, a precise diagnosis of osteosarcoma malignancy needs groundwork of not less than fifty histology slides for portraying a big 3D tumor [7]. Because of the increase of cancer occurrence and sick person-particular medicament choices, detection and medicament of cancer have become additionally intricate [8]. Pathologists should dedicate an exceedingly lengthy time investigating a myriad of slides. Identifying subtle variations of histological images could remain arduous [9]. Misdetection frequently happens because of the substantial job, which lessens the detection's precision. The osteoblasts'

¹Department of Computer Science and Engineering, FEAT, Annamalai University, Chidambaram.

¹Department of Computer science and Engineering, Koneru Lakshmaiah Education Foundation.

²Associate Professor, Department of Computer Science and Engineering, FEAT, Annamalai University, Chidambaram.

^{*3}Associate Professor, School of Computer Science and Engineering, Vellore Institute of Technology, Vellore, India.

Professor and HOD, Department of CSE, Guntur engineering College, AP, India

Email id: ¹ ananddama92@gmail.com, ²

arulselvidhanasekaran@gmail.com

^{*3} balaji.gnb@gmail.com, ⁴rajeshchandra@gmail.com

morphology possesses a slight disparity in distinguished cells that turn the image hardly differentiable. As well, the biopsy remains a significant and time-taking phase for defining the existence of malignant tissue. Meantime, Computer-Aided Detection (CAD) technology provides a resolution for radiologists to automatedly identify malignancies [10]. For handling these constraints, the microscopic image-based assessment remains the basis of cancer detection in the last few years. Nevertheless, it remained impractical prior to the 2000s due to comparatively less diagnosis precision. CAD's bad execution turned medical applications impracticable till the latest developments in computerized image identification [11]. Latest developments facilitated the feasibility of transforming histological slides into digital databases where machine learning (ML) could interfere with digital images for addressing a few constraints.

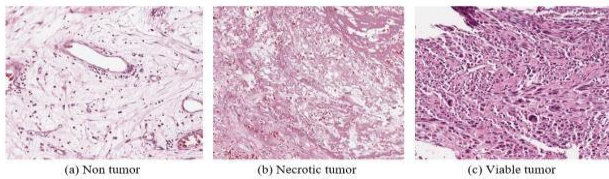


Figure-1 classes of bone tumor using histopathological images

Owing to the emergence of whole slide imaging (WSI), digital pathology turned into a portion of the customary process in medical prognosis. The advent of digital pathology gives a novel perspective of evolving novel algorithms and software. A histological image could be computed in a system like this for enhancing the pathological processes. The system digitalizes glass slides with stained tissue portions at more high-resolution images that turn computerized image assessment feasible and functional [12]. Past medicines remain physical and clinical related. Such traditional classifying techniques have a few impediments such as [13]: Slow diagnostic cycle. Cancer forecast dependent on neurotic reports, which may build the patient's efficacy. For malignancy like cancer, classifying and forecasting require different kinds of medical courses.

According to this discourse, this remains good to possess a system like this, which will facilitate diagnosing and avoiding cancer in the initial phase. This could raise the existence rates for the persons who will adopt cancer [14]. To diagnose cancer by a doctor might turn arduous by observing human bodies till their cells are medicated. Additional study remains necessary for detecting and predicting cancer in the human body. In this day and age, different ML techniques will be used. Such frameworks can distinguish and order malignant growth images that are called cancer images or information of patients like age and symptoms. Machine learning isn't new in the field of examination on malignant growth such as cancer. Henceforth Machine Learning can execute numerous computational astute methods for the forecast of disease. In the perspective of giving finer therapy to the sick person, it remains imperative for definitely prognosticating the diverse cancer kinds [15].

It is a kind of man-made artificial intelligence that centers around the improvement of PC programs which could change when exposed to new data. It utilizes PC models and data got from past and past information to help processes of classification, prediction, and detection.

Feature dimensions can be diminished utilizing the proper feature selection or feature extraction strategy. There are a few

techniques used to decrease the components of features in a dataset. Feature selection methods include choosing a subset of features [16]. Feature extraction then again targets producing new Features by blending the first Features. This denotes their changing Features to a fake set, known as an artificial set, holding still previous dataset's data. Features can impact a machine learning model and its performance. This work aims as follows, that despite a truth that histopathology bone image classification is most important for the diagnosis of malignant growth such as cancer in bones, in both male and female, there is presently no thesis paper concerning ensemble learning (machine) classification with better precision. So, it is imperative to plan a calculation that should be incredibly precise as persons' lives would be in query. ML techniques draw near, with attention on deep learning computations, which have specifically established beneficial appropriateness in medical image examination in the region of nuclear medicine. Although, the classification accuracy of bone cancer, dissected by machine-learning approaches is investigated below.

This paper consists of the ensuing segments: Segment 1 represents the outline of bone cancer, the function of Histopathology in cancer diagnosis, and the implementation of ML in cancer detection, Segment 2 exhibits the present schemes for cancer prognosis with its limitation, Segment 3 provides the feature extraction model, Segment 4 presents the productive experimental assessment, and Segment 5 sums up with a conclusion and upcoming study.

2. Literature Survey

Some of the authors described various classifications in the learning (machine) process which is indicated as follows. Zhao et al. [17] found the Giant cell cancer of bone (GCTB) identification methodology by utilizing Mueller Matrix Polarization Microscopic (MMPM) imaging. Initially, GCTB tissues were classified and examined for the effectiveness of MMPM with its imaging. This method is then applied to model Multi-Parameters Fusion Network (MPFN). By incorporating the defect of this method, Ngoc-Huynh Ho et al. [18] found Regenerative Semi-Supervised Bidirectional W-network (RSS-BW). The classification outcome of dual-phase correlated with solo-phase shows lifting of mean accuracy by 1:7%. The limitation is there are no more data are collected, even then there are poor results in the rate of prediction. The author named Ellmanna et al. [19] constructed a Model-averaged Neural Network (avNNet) to detect initial metastatic illness. Elbashir et al. [20] found a weightless Convolutional Neural Network (CNN) framework for breast cancer classification. Gray-Level Co-occurrence Matrix (GLCM)-related CNN was rather explored by Tan et al. [21]. The authors, Dhillon et al.[22], suggested Extreme Learning Machine (ELM) based model in search of the wake of getting breast cancer survival prediction. It integrates the genomic as well as pathological image datasets. The limitation is, for the survival rate assessment, this method does not consider pathological images when breast cancer patients' survival rate prognosis. CNN was framed by Zhang et al. [23] for pulmonary

Modules' classification. Apart from ensemble classification, Kourou et al. [24] introduced Machine Learning-based (ML) with 10-fold stratified cross-validation to predict lymphoma. But, the drawback was no exploitation of large and

heterogeneous datasets. Finally, Yin et al. [25] introduced Computer-Aided Diagnosis (CAD) at all to help radiologists in bone scintigraphy detection by Characteristic-Point-based Fuzzy Inference System (CPFIS) concerning asymmetry as well as brightness (image) of expert knowledge. The limitation is low accuracy and sensitivity.

3. Methodology

In this section, an extreme machine learning classification to detect bone cancer with five algorithms like support vector machine, logistic regression, Naïve Bayes, K-nearest neighbor, and decision tree. These classifiers will be evaluated using the F-measure parameter and, hence, the voting mechanism is followed. As a result, it is expected to classify the type of cancer such as Osteochondroma, Enchondroma, Aneurysmal bone cyst.

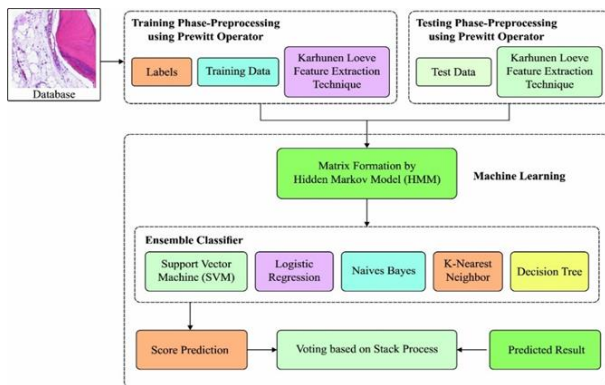


Figure 2: Architecture diagram of the method introduced

Way it has been shown in the figure-3, histopathology bone images are available in the database case, which is classified as the training and testing phase. Then, they are given to Prewitt operator-based pre-processing. This operator reduces unwanted noises and detects the image edges. The pre-processed image is fed into machine learning architecture with a 10-fold cross assessment. The output of the operator is arranged in matrix form and, hence, given to the hidden Markov model, which results in probabilities set. These results are given to the ensemble classifier, which is selected based on their f-measure score. As a result, scores are predicted, and voting is done based on a process known as the stacking process.

3.1 Preprocessing and edge detection using Prewitt operator

In the pre-processing phase, noise oppression remains an essential work. Noise decrement remains a significant and fundamental portion of the remote processing of sense images. When we talk of noise, we get that it leads to pixel values, which in no way imitates the actual scene's true intensities. Prewitt operator is an approximate means to calculate the magnitude and edge orientation. Equations using by Prewitt operator are given below, the constant $k = 1$. This Prewitt operator doesn't place at all any emphasis on pixels that are nearer to the center of masks. This particular method undergoes two will measure constituents such as vertical and horizontal methods, whereas the vertical with the kernel is indicated as $V(i)$ and horizontal with kernel component is indicated as $H(j)$. $|V(i)| + |H(j)|$ give a sign of gradient intensity in the current pixel. As a result, the

combination of these components contains a couple of 3×3 convolution kernels. One kernel remains just the other turned by 90° .

The kernels remain so considered to rejoin majorly and could be implemented individually to input picture (image) to generate separate dimensions of gradient elements within every orientation, that is., $V(i)$ and $H(j)$. These could be later amalgamated for seeking an absolute gradient magnitude at every point.

$$|\Delta X| = |V2(i)| + |H2(j)| \quad (1)$$

Angle of edge orientation with spatial gradient is denoted as,

$$\text{Angle } (\Delta X) = \tan^{-1} \frac{V(i)}{H(j)} \quad (2)$$

The computation of image gradient is dependent on obtaining partial derivatives at each pixel, and hence, grey levels are obtained from the image.

3.2 Process of Feature extraction

Now, edges of images are detected assuredly and Karhunen-Loeve (KL) is used in feature extraction. This Karhunen-Loeve (KL) is a sheer projection-based technique, in which a particular technique facilitates a reduction in dimension of data employing constructing orthogonal principal components that are weighted. Assuming that an edge detected rather a linear transformation mapping process of aboriginal N-dimensional feature space into an M-dimensional space, where $M < N$, the transform can be denoted as follows:

$$D_{m,n} = DVX_a \quad (3)$$

Where, DV indicates eigenvector, whose length depends on the components which are required to find the observation feature space.

$D_{m,n}$ is the total dimension of M and N.

X_a is space as a result.

Feature Space that is left as a result is as a projection of data original and such a set over eigenvectors of the covariance matrix. The feature extraction is comprised of the following steps:

Step-1: Absolutely original matrix is transmuted into a standardized matrix.

Step-2: Next, the covariance matrix is to be calculated. Eigenvalues, as well as corresponding Eigenvectors of the covariance matrix, are computed.

Step-3: Eigenvector with maximum Eigenvalue is the first principle component consisting of most significant data.

Step-4: Initial few principal components are chosen to be contributions of classifiers.

3.3 Architecture of classification network

The training dataset is separated randomly into X equal size subsets. If we have Y samples, at that point size of every subset will be (X/Y) . To expand numerableness among remade training datasets, each new training set (TS) is acquired through resampling on X-1 out of X subsets. At that spot, training with every subset is finished utilizing one out of three base classifier learners, which is chosen haphazardly. A trained classifier is added to the group and the cycle is rehashed for the rest of the

subsets. In the following iteration, the variety, as well as precision of collection that is at present, is improved with the expansion of Ek (ensemble number), at that spot, it will be held in an upgraded ensemble and prohibited otherwise.

3.4 Extreme machine learning classification method

The outcomes of the classification of the 3 finest classifiers will be provided to the ensemble classification technique that gives the last characterization result. Subtleties of classification paradigms and voting mechanisms utilized will be provided in the ensuing sub-segments.

3.4.1 Hidden Markov Model (HMM) for Support vector machine

The covered-up Markov model accomplishes mitigation of time complexity and increases in the analysis of confidence level when contrasted with customary classifiers. HMM has three following stochastic matrices:

Transition matrix, A, of changing probabilities is as changing from one state to some other. There is a likelihood of changing, which from state I to state j is indicated by bij.

The initial distribution vector, π, is rather a column vector that stores likelihoods of beginning in each state toward the start of the sequence. πi indicates the probability of beginning in state i. In the end, observation matrix, B, characterizes the likelihoods of observing each base pair for each state. The likelihood of observing observation k in state j is indicated by aj(k).

3.4.2 Logistic regression

The Logistic Regression classification paradigm remains a favorite selection modeling binary classification. For this paradigm, the conditional probability of one among the 2 output classes remains to be equivalent to a linear blend of input histopathology features. The logistic equation utilized for this classification paradigm remains:

$$LR(i) = \ln \frac{m(i)}{1-m(i)} \quad (4)$$

where m remains the probability of the event i's happening.

3.4.3 Naïve Bayes

The posterior probability is available for each class. Such posterior probability of each class is calculated. The equation below performs the Naïve Bayes formula.

$$P(c_i/v_1, v_2 \dots v_n) = \frac{p(c_i) \prod_{j=1}^n p(v_j/c_i)}{p(v_1, v_2 \dots v_n)} \quad (5)$$

P(c_i/v₁, v₂...v_n) is the probability of feature extracted image with its respective class Ci, and this Ci should be less than v, where, v= v₁, v₂...v_n which is an observed instance. Samples were divided into ten randomly generated subsets later. Further, a tenfold cross-validation method dependent on the Naïve Bayes model was all utilized to train the algorithm on ninefold and test it on remaining onefold rather.

K-nearest neighbor

KNN algorithm will be applied by incorporating S = (xi, yi), i = 1, 2, ...Nis TS deemed, where xi is d-dimensional feature vector, and yi ∈ {+1, -1} is combined with experimental class tags. For

the sake of easiness, we suppose a binary classification. Usually, we assume the entire training datasets are with its random variables (X,Y) that are distributed anonymously. With the earlier considered samples, as TS S, the KNN algorithm builds a native sub-area R(x) ⊆ Rd of the input gap that will be positioned at such a spot as an approximation note x. Predicting region R(x) consists of nearest training points to x, which is engraved as given below:

$$R(x) = \{x. D(x, x') \leq d(k)\} \quad (6)$$

in which, D(x, x') is distance metric, k indicates the count of features in region R(x)

Likelihood of posterior is indicated as P(y/x)

$$P(y/x) = \frac{p(x/y)p(y)}{p(x)} \quad (7)$$

Where p(x/y) is the feature extracted histopathology image.

3.4.4 Decision tree

The TS feature extracted images will be selected to turn common with the feature behavior concerned with the criteria also for identifying data acquiring for diverse feature arrays. Features having elevated data acquiring will be selected as decision tree features.

3.4.6 Algorithm

Input: histopathology bone images (Z), training dataset (i), testing dataset(j)

Output: classified region(x)

1. Preprocess and edge detection (ED): Apply perwitt operator in i and j

2. Compute: vertical component V(i,j) and component H(i,j) horizontal

3. Estimate ΔX,

$$|\Delta X| = |V2(i)| + |H2(j)|$$

4. compute angle,

$$\text{Angle } (\Delta X) = \tan^{-1} \frac{V(i)}{H(j)}$$

5. Zfe ← Zed

6. Feature extraction (Zfe): M*N, M<N

Dm,n = DV Xa, (Zed)

Step-1: original matrix [0,1]

Step-2: covariance matrix: W(Dm,n)

Step-3: compute its variance

7. Zen ← Zfe, subset (X/Y)

Generate m(i) from equation (4) with m is likelihood of every event (i)

Generate P(c_i/v₁, v₂...v_n) from equation (5), Ci < v

Estimate 10 fold validation

Generate S = (xi, yi), i = 1, 2, ...N from equation (6)

Predict ROI R(x)

Generate root along with internal node

8. Compute voting process in Zen = { Zen 1', Zen 2', ... Zen 5'}

$$\text{Estimate: } P(\text{Zen}) = \frac{\sum_{i=1}^5 \text{label}(\text{Zen})}{5}$$

P(Zen) ← x

9. Classified region (x)

3.5 Prediction process

For five classification models, Zen' is fragmented into five innovative disjoint subsets { Zen 1', Zen 2',... Zen 5'}; 5 subsets are inclined to the TS, and then, the remainder form will be utilized for testing. Such performing is ensued in carrying out classification jobs for every ML model rather. In the end, each image (xi,j) in the database (D) could reach a forecast outcome; for Stack Based Voting (SBV), novel database D' would be employed as input for fusion networks for performing immediate end classification outcomes. In voting, the prognosticated class label for a specific sample remains the class label, which signifies the maximum of class labels projected by every independent classifier.

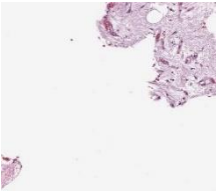

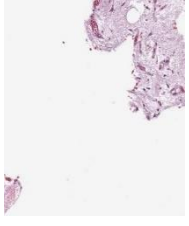
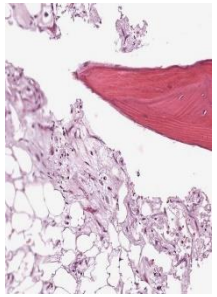
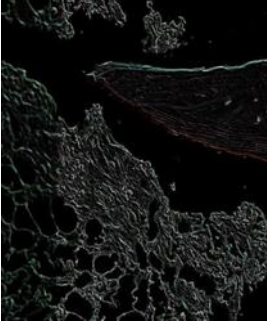
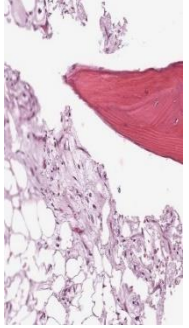
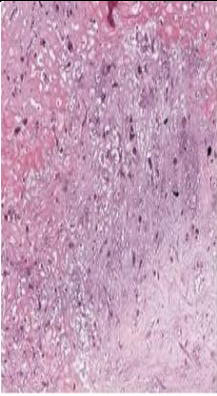

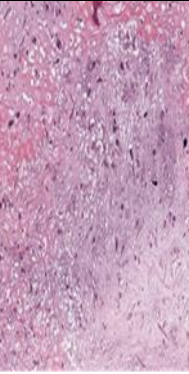
$$P(\text{Zen}) = \frac{\sum_{i=1}^5 \text{label}(\text{Zen})}{5} \quad (8)$$

in which P(Zen) remains the end prognosis outcome for image (Zen) utilizing the voting methodology, and it can be identified as Osteochondroma, Enchondroma, Aneurysmal bone cyst, and Chondroblastoma.

4. Performance Analysis

The proffered methodology will be assessed upon 2 renowned publically accessible bone Histopathology databases. They chose forty WSIs of the digitalized images portraying humor heterogeneousness and reply characteristics in the research. In every WSI, thirty 1024×1024 pel image tiles have been haphazardly chosen at the 10X magnification feature. Subsequent to eliminating impertinent tiles, 1,144 of the consequential 1,200 image tiles, like those that come under non-fabric, ink marks areas, and blurry images, have been selected. This algorithm contrasts with the prevailing algorithms concerning diverse criteria such as accuracy, sensitivity specificity, f1 score, and recall that are selected. To confirm that the suggested Deep Convolutional Extreme Learning Machine (DC-ELM) algorithm is more effectual when compared with the prevailing methodologies, the graphs are provided here. For simulation herein, we selected PYTHON.

Table 1: Various Stages to Process the three classes of histopathological images of Bone Cancer

Input Image classes		Pre-Processed	Output Image
	Necrotic Tumour		
	Non- Tumor		
	Viable - Tumor		

The above table 1 limits all the possibilities of processing the histopathological images. It is all with an assessment to detect how the suggested Deep Convolution Extreme Learning Machine (DC-ELM) algorithm functions, which consists of five metrics like accuracy, recall, precision, sensitivity, and specificity. Using true positive (TP), true negative (TN), false negative (FN), as well as false positive (FP), we are getting the

following calculation.

If Sensitivity refers to the detectability to precisely diagnose cancer in the database, the sensitivity computation does not consider indeterminate test outcomes as a test could not be reiterated, and intermediary samples must be entirely omitted out of the assessment.

$$\text{Sensitivity} = \frac{TP}{TP+FN} \quad (9)$$

Table 2 presents the Sensitivity assessment with the prevailing 3D-GLCM CNN and CNN with gene data as well as RSS-BW with the proffered DC-ELM .

Table 2: Sensitivity assessment

Number of epochs	3D-GLCM CNN (%)	CNN with gene data(%)	RSS-BW(%)	DC-ELM (%)
100	84	86	95.6	96.39
200	88	89	96.69	97.24
300	90	92	98	98.20
400	93	94	98.4	99.57
500	95	96	98.93	99.62

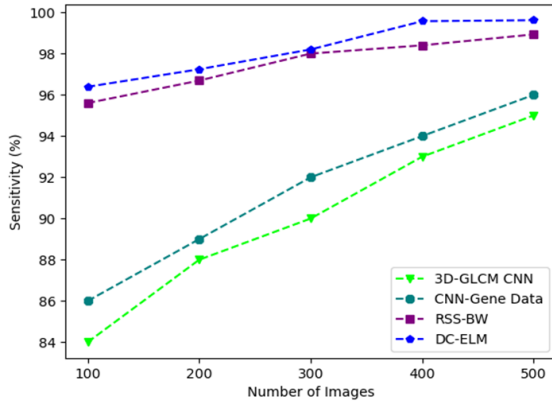


Figure 3: Sensitivity correlation

Figure 3 illustrates the sensitivity correlation of the prevailing and proffered algorithms. The X-axis and the Y-axis show the epoch's quantity and sensitivity in percentage accordingly. The sensitivity of the proposed DC-ELM algorithm attains finer execution when compared with the prevailing methodologies. Specificity refers to the identification capability to rightly decline non-cancer parts in the dataset. Arithmetically, this could as well be provided as,

$$\text{Specificity} = \frac{TN}{TN+FP} \quad (10)$$

Table 3 presents Specificity Analysis with existing 3D-GLCM CNN and CNN with gene data as well as RSS-BW with the proffered DC-ELM .

Number of epochs	3D-GLCM CNN(%)	CNN with gene data(%)	RSS-BW(%)	DC-ELM (%)
100	68.45	93.35	97.74	98.88
200	69.75	94.78	98.38	99.36
300	70.45	95.89	98.47	99.85
400	73.5	97.57	99.06	99.86
500	74.69	98.74	99.38	99.89

Table 3: Specificity assessment

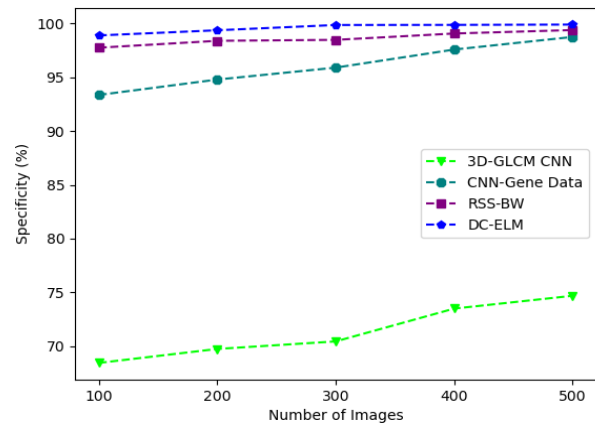


Figure 4: Specificity Correlation

Figure 4 illustrates the sensitivity correlation of the prevailing and proffered algorithms. The X-axis and the Y-axis show the epoch's quantity and specificity in percentage accordingly. The specificity of the proposed DC-ELM algorithm attains 99.89% for 500 images, which shows that it is a finer execution when compared with the prevailing methodologies.

Accuracy remains the right prognoses quantity divided by predictions made overall. Arithmetically, this is provided as,

$$\text{Accuracy} = \frac{TP+TN}{TP+TN+FP+FN} \quad (11)$$

Table 4 provides the assessment of the accuracy with the existing 3D-GLCM CNN and CNN with gene data and RSS-BW with the proffered DC-ELM .

Number of epochs	3D-GLCM CNN(%)	CNN with gene data(%)	RSS-BW(%)	DC-ELM (%)
100	88.45	93.88	94.37	95.42
200	90.69	94.56	94.98	96.83
300	92.34	95.84	96.77	97.3
400	92.35	96.34	97	97.46
500	93.03	97.83	98.79	99.34

Table 4: Accuracy assessment

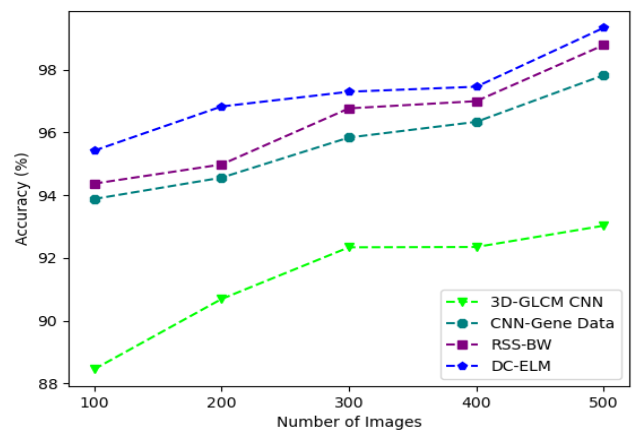


Figure 5: Accuracy correlation

Figure 5 illustrates the accuracy correlation of the prevailing and proffered algorithms. The X-axis, as well as the Y-axis, show the epoch's quantity and sharp accuracy in percentage respectively.

Absolute accuracy of the suggested DC-ELM algorithm achieves higher accuracy than existing algorithms.

The rate of precision is the proportion of the positive sample number. Instead, precision portrays the ratio of the prognosis paradigms of cancer in which cancer really exists. The rate of precision (P) is described by:

$$\text{Precision} = \frac{TP}{TP+FP} \quad (12)$$

Table 5 provides the precision assessment with the prevailing 3D-GLCM CNN and CNN with gene data and RSS-BW with the proffered DC-ELM algorithm.

Table 5: Precision assessment

Number of epochs	3D-GLCM CNN(%)	CNN with gene data(%)	RSS-BW(%)	DC-ELM (%)
100	67.78	77.87	78.65	84.67
200	68.98	78.88	79.85	85.63
300	72.67	81.93	83.67	88.47
400	73	82.74	85.67	89.63
500	73.57	83.76	89.45	90.76

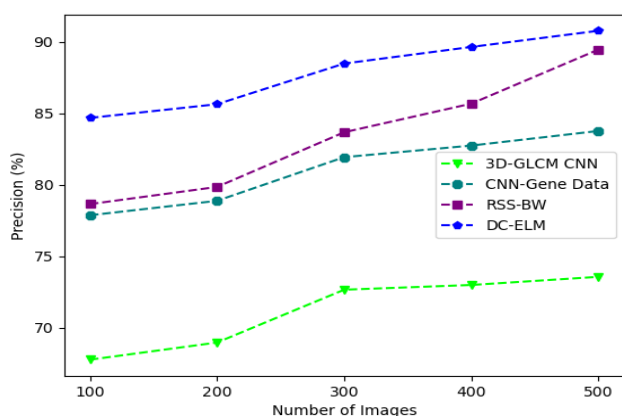


Figure 6: Precision correlation

Figure 6 illustrates the precision correlation of the prevailing and proffered algorithms. The X-axis and the Y-axis show the epoch's quantity and precision in percentage accordingly. The precision of the proposed DC-ELM algorithm achieves further results when compared with the prevailing algorithms.

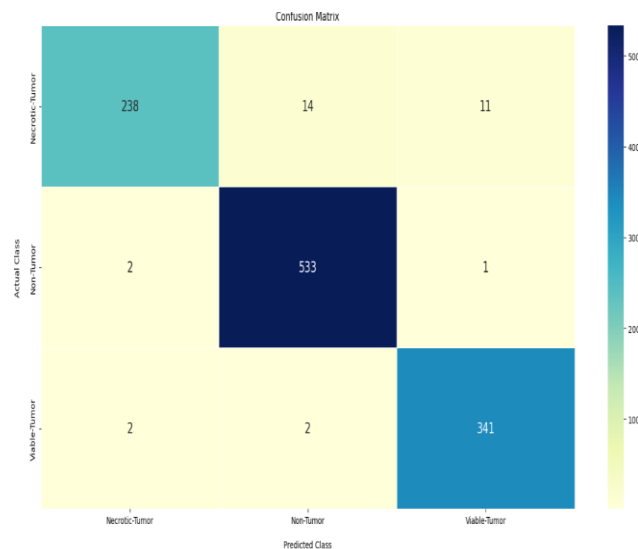


Figure 7: analysis of confusion matrix

Figure 7 illustrates the confusion matrix for features employing the classifier training model where the rows portray the prognosticated class (output class) and columns portray the real class (target class) of data concerning the attack. The cross-wise black, blue, and grey cells indicate the trained networks, which remain rightly and wrongly classified. The column upon the right denotes each prognosticated real class whereas the row below portrays the execution of each real class.

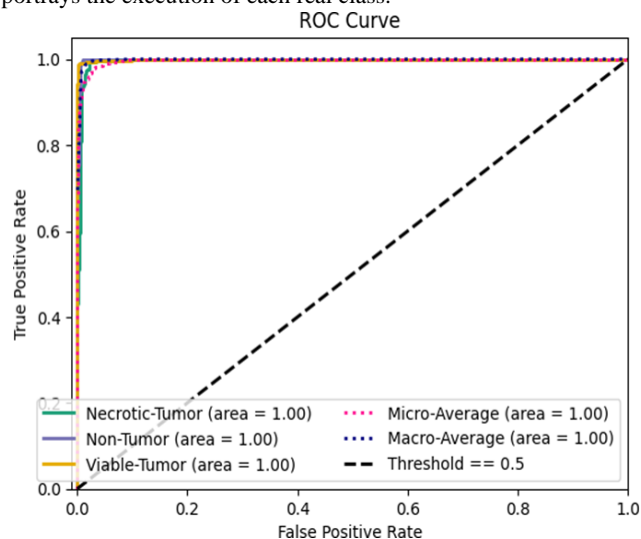


Figure 8: Analysis of ROC

Figure 8 indicates the comparison of ROC, where the X-axis portrays the false positive rate and the Y-axis portrays the true positive rate. It is found that the area for the necrotic tumor is 1, the area of non-tumor is 1, and the area of the viable tumor is 1 with the micro/macro average area in 1 and threshold level is 0.5.

Table 6 illustrates the execution of the assessment for the proffered DE-CLM for the classes such as necrotic-tumor, non-tumor, and viable tumor. It is found that the proffered methodology attains 97.2% of accuracy, 96.26% of sensitivity, and 98.47% of specificity.

Table 7 shows the comprehensive execution of assessment for prevailing 3D-gray-level co-occurrence matrix (3D-GLCM CNN), Convolutional Neural Network (CNN) with gene data, and Regenerative Semi-Supervised Bidirectional W-network (RSS-BW) with the proffered Deep Convolutional Extreme Learning Machine (DC-ELM). The criteria regarded for assessment remains sensitivity, specificity, accuracy, and precision.

Table-6 comparative analysis for various classes of tumor

Class	Accuracy	Sensitivity	Specificity
Necrotic-Tumor	0.9747	0.9049	0.9955
Non-Tumor	0.9834	0.9944	0.9737
Viable-Tumor	0.986	0.9884	0.985
Overall	0.972	0.9626	0.9847

Table 7: Comprehensive execution assessment

Methodology	Sensitivity (%)	Specificity (%)	Accuracy (%)	Precision (%)
3D-GLCM CNN [14]	90	71.368	91.371	71.2
CNN with gene data [13]	91.4	96.066	95.69	81.036
RSS-BW [11]	97.52	98.606	96.382	83.458
DC-ELM (Proposed)	98.204	99.568	97.27	87.832

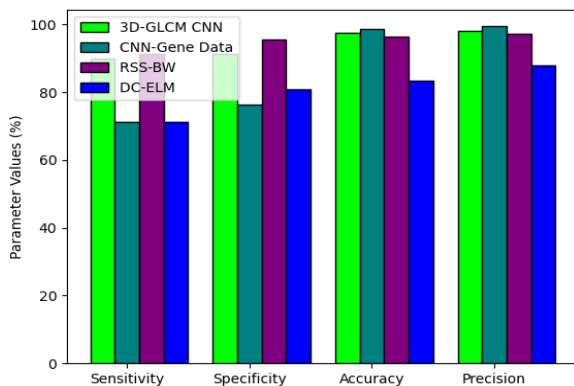


Figure 9: Comprehensive comparative assessment of prevailing and proffered algorithms.

Figure 9 correlates the values attained for the criteria. The X-axis and Y-axis show parameters considered for analysis and their values are attained in percentage accordingly. The proffered algorithm attains 98.2% of sensitivity, 99.56% of specificity, 97.27% of accuracy, and 87.83% of precision. Lastly, while correlated with the existing 3D-GLCM CNN and CNN with gene data and RSS-BW, the proffered DC-ELM algorithm exhibits finer outcomes.

5. Conclusion

Bone cancer causes unnatural growth of cells to proliferate delinquently in the bone that, instead, demolish ordinary bone

tissues and start to expand in the rest of the body parts. Identifying cancer tissue remains a critical problem for pathologists for understanding and detecting possible lesion tissue. This study describes a Deep Convolutional Extreme Learning Machine (DC-ELM) to predict knee bone's cancer state from Histopathology images and demonstrate an apt model performance by using training and testing images. As a result, the proposed DC-ELM algorithm achieves 98.2% of sensitivity, 99.56% of specificity, 97.27% of accuracy, and 87.83% of precision. For future work, there is a plan to construct a new convolutional deep learning architecture with an optimization algorithm to improve accuracy, precision, and recall.

References

- [1] Nisthula P andYadhu.R.B, "A Novel Method to Detect Bone Cancer using Image Fusion and Edge Detection", Proceedings of Engineering and Computer Science, vol.3, no.2, pp.2012- 2018, 2013.
- [2] Hubert H. Chuang, Beth A. Chasen, and TinsuPan, "Bone Cancer Detection from MRI Scan Imagery Using Mean Pixel Intensity", Proceedings of Advanced Research in Computer and Software Engineering, vol.1, no.5, pp.1-7, 2013.
- [3] Balaji, G. N., T. S. Subashini, and A. Manikandarajan. "Automatic Classification of Anterior-Posterior and Lateral Views of Leg X-rays", International Research Journal of Engineering and Technology (IRJET), Vol.2, no.9, pp.968-974, 2015.
- [4] Tume-Bruce, B. A. A. ., A. . Delgado, and E. L. . Huamaní. "Implementation of a Web System for the Improvement in Sales and in the Application of Digital Marketing in the Company Selcom". International Journal on Recent and Innovation Trends in Computing and Communication, vol. 10, no. 5, May 2022, pp. 48-59, doi:10.17762/ijritcc.v10i5.5553.
- [5] Balaji, G. N., T. S. Subashini, and N. Chidambaram. "Cardiac view classification using speed Up robust", Indian Journal of Science and Technology, Vol.8, no.7, pp.1-5,2015.
- [6] Jayashree Dev, Sanjit K Dash, Sweta Dash, and Madhusmita Swain, "A Classification Technique for Microarray Gene Expression Data using PSOFLANNI", International Journal on Computer Science and Engineering (IJCSE), vol.4, no.9, pp.1534-1539, 2012.
- [7] K. Simonyan, A. Zisserman, Very deep convolutional networks for large-scale image recognition, arXiv preprint arXiv:1409.1556 (2014).
- [8] C. Szegedy, W. Liu, Y. Jia, P. Sermanet, S. Reed, D. Anguelov, D. Erhan, V. Vanhoucke, A. Rabinovich, Going deeper with convolutions, in: Proceedings of the IEEE conference on computer vision and pattern recognition, 2015, pp. 1–9.
- [9] Gupta, D. J. . (2022). A Study on Various Cloud Computing Technologies, Implementation Process, Categories and Application Use in Organisation. International Journal on Future Revolution in Computer Science & Communication Engineering, 8(1), 09–12. <https://doi.org/10.17762/ijfrcsce.v8i1.2064>
- [10] H.-C. Shin, H. R. Roth, M. Gao, L. Lu, Z. Xu, I. Nogues, J. Yao, D. Mollura, R. M. Summers, Deep convolutional neural networks for computer-aided detection: Cnn architectures, dataset characteristics and transfer learning, IEEE transactions on medical imaging 35 (2016) 1285–1298.
- [11] W. Rawat, Z. Wang, Deep convolutional neural networks for image classification: A comprehensive review, Neural computation 29 (2017) 2352–2449. [
- [12] A. Serag, A. Ion-Margineanu, H. Qureshi, R. McMillan, M.-J. Saint Martin, J. Diamond, P. O'Reilly, P. Hamilton, Translational ai and deep learning in diagnostic pathology, Frontiers in Medicine 6 (2019)
- [13] N. Wahab, A. Khan, Y. S. Lee, Transfer learning based deep cnn

for segmentation and detection of mitoses in breast cancer histopathological images, *Microscopy* 68 (2019) 216–233.

- [14] M. Yanagawa, H. Niioka, A. Hata, N. Kikuchi, O. Honda, H. Kurakami, E. Morii, M. Noguchi, Y. Watanabe, J. Miyake, et al., Application of deep learning (3-dimensional convolutional neural network) for the prediction of pathological invasiveness in lung adenocarcinoma: A preliminary study, *Medicine* 98 (2019).
- [15] KonstantinaKourou, Themis P. Exarchos, Konstantinos P. Exarchos, Michalis V. Karamouzis, Dimitrios I. Fotiadis, “Machine Learning Applications in Cancer Prognosis and Prediction”, *ELSEVIER Computational and Structural Biotechnology Journal*, vol.13, pp.8-17, 2015.
- [16] Maulik U, Chakraborty D, “Fuzzy preference based feature selection and semisupervised SVM for cancer classification”, *IEEE Trans NanoBiosciences*, vol.13, no.2, pp.152-160, 2014.
- [17] V. JothiPrakash and L.M.Nithya, “A Survey on Semi-Supervised Learning Techniques”, *International Journal of Computer Trends and Technology (IJCTT)*, vol.8, no.1, pp.25-29, 2014.
- [18] Y. Celik, M. Talo, O. Yildirim, M. Karabatak, U. R. Acharya, Automated invasive ductal carcinoma detection based using deep transfer learning with whole-slide images, *Pattern Recognition Letters* (2020).
- [19] Zhao, Yongqiang, Mohamed Reda, Kai Feng, Peng Zhang, Gaojian Cheng, ZhigangRen, Seong G. Kong, Shihan Su, HaiXia Huang, and Jiyuan Zang, “Detecting Giant Cell Cancer of Bone Lesions Using Mueller Matrix Polarization Microscopic Imaging and Multi-Parameters Fusion Network”, *IEEE Sensors Journal*, vol.20, no.13, pp.7208-7215, 2020.
- [20] Ho, Ngoc-Huynh, Hyung-Jeong Yang, Soo-Hyung Kim, Sung Taek Jung, and Sang-Don Joo, “Regenerative Semi-Supervised Bidirectional W-Network-Based Knee Bone Cancer Classification on Radiographs Guided by Three-Region Bone Segmentation”, *IEEE Access*, vol.7, pp.154277-154289, 2019.
- [21] Kiran, M. S., & Yunusova, P. (2022). Tree-Seed Programming for Modelling of Turkey Electricity Energy Demand. *International Journal of Intelligent Systems and Applications in Engineering*, 10(1), 142–152. <https://doi.org/10.18201/ijisae.2022.278>
- [22] Ellmann, Stephan, Lisa Seyler, Jochen Evers, HenrikHeinen, AlineBozec, Olaf Prante, TorstenKuwert, Michael Uder, and Tobias Baeuerle, “Prediction of early metastatic disease in experimental breast cancer bone metastasis by combining PET/CT and MRI parameters to a Model-Averaged Neural Network”, *Bone*, pp.254-261, 2019.
- [23] Elbashir, Murtada K, Mohamed Ezz, Mohanad Mohammed, and Said S. Saloum, “Lightweight Convolutional Neural Network for Breast Cancer Classification Using RNA-Seq Gene Expression Data”, *IEEE Access*, vol.7, pp.185338-185348, 2019.
- [24] Tan, Jiaying, YongfengGao, Zhengrong Liang, Weiguo Cao, Marc J. Pomeroy, YumeiHuo, Lihong Li, Matthew A. Barish, Almas F. Abbasi, and Perry J. Pickhardt, “3D-GLCM CNN: A 3-Dimensional Gray-Level Co-Occurrence Matrix-Based CNN Model for Polyp Classification via CT Colonography”, *IEEE transactions on medical imaging*, vol.39, no.6, pp.2013-2024, 2019.
- [25] Dhillon, Arwinder and Ashima Singh, “eBreCaP: extreme learning-based model for breast cancer survival prediction”, *IET Systems Biology*, vol.14, no.3, pp.160-169, 2018.
- [26] Zhang, Baihua, Shouliang Qi, Patrice Monkam, Chen Li, Fan Yang, Yu-Dong Yao, and Wei Qian, “Ensemble learners of multiple deep CNNs for pulmonary nodules classification using CT images”, *IEEE Access*, vol.7, pp.110358-110371, 2018.
- [27] Linda R. Musser. (2020). Older Engineering Books are Open Educational Resources. *Journal of Online Engineering Education*, 11(2), 08–10. Retrieved from <http://onlineengineeringeducation.com/index.php/joe/article/view/41>
- [28] Kourou, Konstantina D, Vasileios C. Pezoulas, Eleni I. Georga, Themis Exarchos, Costas Papaloukas, MichalisVoulgarelis, and Andreas Goules, “Predicting Lymphoma Development by Exploiting Genetic Variants and Clinical Findings in a Machine Learning-Based Methodology With Ensemble Classifiers in a Cohort of Sjögren's Syndrome Patients”, *IEEE Open Journal of Engineering in Medicine and Biology*, vol.1, pp.49-56, 2018.
- [29] Yin, Tang-Kai and Nan-TsingChiu, “A computer-aided diagnosis for locating abnormalities in bone scintigraphy by a fuzzy system with a three-step minimization approach”, *IEEE Transactions on Medical Imaging*, vol.23, no.5, pp.639-654, 2014.
- [30] Anand, D., Arulselvi, G., Balaji, G.N. (2022). An Assessment on Bone Cancer Detection Using Various Techniques in Image Processing. In: Deepak, B.B.V.L., Parhi, D., Biswal, B., Jena, P.C. (eds) *Applications of Computational Methods in Manufacturing and Product Design*. Lecture Notes in Mechanical Engineering.

Acknowledgements

This research was supported/partially supported by [Department of Computer science and Engineering, Koneru Lakshmaiah Education Foundation]. We thank our colleagues from [Annamalai university, Vellore Institute of Technology, Guntur engineering College] who provided insight and expertise that greatly assisted the research, although they may not agree with all of the interpretations/conclusions of this paper. We thank [G.Arul Selvi, G.N.Balaji] for assistance with [methodology], and [G RAJESH CHANDRA] for comments that greatly improved the manuscript.

Author Contributions

Anand Dama: Conceptualization, Methodology, Software, Field study

Arul Selvi G: Data curation, Writing-Original draft preparation, Software, Validation., Field study

Balaji GN: Visualization, Investigation, Writing-Reviewing

G RAJESH CHANDRA: Editing.

Conflicts of Interest

The authors declare no conflicts of interest.